JACS
JOURNAL OF THE AMERICAN CHEMICAL SOCIETY
Article
pubs.acs.org/JACS

Chemical Noise Produced by Equilibrium Adsorption/Desorption of Surface Pyridine at Au−Ag−Au Bimetallic Atom-Scale Junctions Studied by Fluctuation Spectroscopy

Tai-Wei Hwang,[†] Sean P. Branagan,[†] and Paul W. Bohn*[,†,‡]

[†]Department of Chemical and Biomolecular Engineering and [‡]Department of Chemistry and Biochemistry, University of Notre Dame, Notre Dame, Indiana 46556, United States

Supporting Information

ABSTRACT: The chemical noise contained in conductance fluctuations resulting from adsorption and desorption of pyridine at Au−Ag−Au bimetallic atom-scale junctions (ASJs) exhibiting ballistic electron transport is studied using fluctuation spectroscopy. ASJs are fabricated by electrochemical Ag deposition in a Au nanogap to produce a high-conductance Ag quantum wire, followed by electromigration-induced thinning in pyridine solution to create stable ASJs. The conductance behavior of the resulting ASJs is analyzed by sequential autocorrelation and Fourier transform of the current−time data to yield the power spectral density (PSD). In these experiments the PSDs from Ag ASJs in pyridine exhibit two main frequency regions: $1/f$ noise originating from resistance fluctuations of the junction itself at low frequencies, and a Lorentzian noise component arising from molecular adsorption/desorption fluctuations at higher frequencies. The characteristic cutoff frequency of the Lorentzian noise component determines the relaxation time of molecular fluctuations, which, in turn, is sensitive to the kinetics of the adsorption/desorption process. The kinetics are found to depend on concentration and on the adsorption binding energy. The junction size ($<5G_0$), on the other hand, does not affect the kinetics, as the cutoff frequency remains unchanged. Concentration-dependent adsorption free energies are interpreted as arising from a distribution of binding energies, $N(E_b)$, on the Ag ASJ. Other observations, such as long lifetime ASJs and two-level fluctuations in conductance, provide additional evidence for the integral role of the adsorbate in determining ASJ reorganization dynamics.

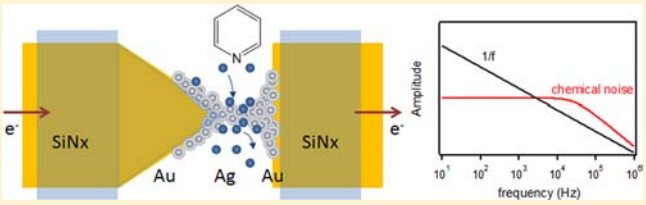

INTRODUCTION

Chemical sensing using metallic nanomaterials such as thin films (2D)[1−5] and nanowires (1D)[6−8] is a subject of intense interest. Upon adsorption of molecular species at nanostructured metal−liquid interfaces, the conductivity of the metallic nanostructure shifts, a phenomenon explained by the Fuchs−Sondheimer model of free electrons with random point scattering.[9,10] As the size of the nanostructure decreases, surface effects become more important, and sensitivity to molecular adsorption is enhanced. An atom-scale junction (ASJ) or quantum wire (QW), consisting of only a few metal atoms at the narrowest point, is the smallest metallic architecture possible, and so exhibits great potential for molecular detection and for fundamental studies of mesoscopic molecular assemblies.

The defining characteristic of metallic ASJs is quantized conductance. Electron transport through ASJs occurs in the ballistic regime, where electrons propagate through the junction without scattering as the dimensions of the ASJ reach the Fermi wavelength. The conductance, G, of an ASJ is commonly expressed as

$$G = G_0 \sum_{i=1}^{N} T_i \quad (1)$$

where $G_0 = 2e^2/h = 77.4\ \mu S = 1/(12.9\ k\Omega)$ is the conductance quantum, e is the electron charge, h is Planck's constant, T_i is the transmission probability of the ith channel, and the summation is taken over all active channels. In the ballistic transport regime the wire length is smaller than both the mean free path and the phase relaxation length of the electron, so $T_i = 1$ and $G = NG_0$.[11,12]

Many groups have reported molecular sensing using ASJs, and the performance is impressive. The earliest sensing work was done by Tao and co-workers, who showed a fast response time and high sensitivity of detection using Cu ASJs.[13,14] They demonstrated molecular adsorption of different species on ASJs, and showed that the adsorbate-induced conductance change, ΔG, depends strongly on the size of the junction and the binding strength of the molecules to the ASJ surface. Smaller junctions and more strongly binding molecules generate larger ΔG values. Other adsorbates, such as cyclodextrin, can play multiple roles, as shown on Cu ASJs.[15] Quantum wires fabricated from other metals, such as Ag and Au, have also been studied. Dong et al. studied NH_3 adsorption on Ag QWs,[16] observing that in aqueous solution the concentration of ammonia and pH strongly affect ΔG. They

Received: January 17, 2013
Published: February 22, 2013

proposed that Ag surface adatoms displaying redox behavior distinct from that of the QW body induce QW structural reorganization, which is manifested as a conductance change. Studies of alkanethiol adsorption on Au ASJs as a function of ASJ native conductance have been carried out in our laboratory. The magnitude of conductance changes was found to be independent of QW conductance and similar to adsorption on thin films for wires displaying $G > 20G_0$;[17] however, smaller wires with $G < 20G_0$ exhibit monotonically increasing sensitivity to molecular adsorption with decreasing wire diameter, and large impedance changes ($\Delta Z/Z_0 \approx 70\%$) have been observed for the smallest ASJs ($G \approx 2-3G_0$).[18]

To date, chemical sensing experiments using ASJs have focused on detecting molecular adsorption by studying the pre- to post-adsorption conductance change through the ASJ. In these experiments, the conductance change, ΔG, is proportional to the change in surface population of a monolayer-forming adsorbate, ΔN. Alternatively, because molecular adsorption at metallic ASJs is subject to molecular fluctuations at equilibrium, signal changes induced by these fluctuations, i.e., chemical noise, are detectable in the mesoscopic realm represented by metallic ASJs. Thus, information about surface adsorption/desorption dynamics can be obtained by direct observation. Under steady-state conditions, Poisson statistics show that, for small populations of $\langle N \rangle$ molecules, the standard deviation is $\langle N \rangle^{1/2}$, where $\langle N \rangle$ is the average population, and the signal-to-noise magnitude also scales as $\langle N \rangle^{1/2}$. Furthermore, the signal-to-noise scaling obtained from this analysis agrees with the theoretical work of Donnan et al. addressing fluctuations in simple chemical equilibria.[19] As the size of QW decreases into the ballistic transport regime, sensitivity, as measured by ΔG, is enhanced,[20] while the surface population, $\langle N \rangle$, is reduced. Combining these two factors, the relative contribution of chemical noise is greatly enhanced in measurements using the smallest ASJs. Moreover, the signal fluctuations at equilibrium can be readily analyzed using fluctuation spectroscopy, as originally developed by Weissman and Feher.[21,22] In a reversible system at equilibrium, fluctuations between two states manifest perturbations that decay as $\exp(-t/\tau)$, where τ is a characteristic relaxation time. The frequency spectrum, or power spectral density (PSD), corresponding to the decay displays a Lorentzian form with cutoff frequency (half-width at half-maximum) $f_c = (2\pi\tau)^{-1}$. Fluctuation spectroscopy has been used to characterize electrochemical experiments,[23−25] but rarely in studying surface population fluctuation.[26,27] Zheng et al. performed surface fluctuation analysis using a silicon nanowire biosensor, and showed excess Lorenztian noise above the background $1/f$ (or $1/f^{\alpha}$) noise.[27] However, in these experiments, the Lorenztian noise could not be definitively assigned to fluctuations of surface biomolecule population, because the spectra remained insensitive to concentration, and the measured cutoff frequency was much higher than the estimated value.

The focus of the work reported here is to demonstrate the feasibility of studying molecular fluctuations at atomic-scale surfaces by applying fluctuation spectroscopy to the electrical signal measured upon pyridine adsorption on the active Ag region of a bimetallic Au−Ag−Au ASJ. It is known that Lewis bases tend to adsorb on noble metals. However, in order for surface molecular fluctuations to be observed, the molecule must possess a significant off-rate, so that both adsorption and desorption occur at measurable rates. Thus, the free energy of adsorption is a key factor in choosing an adsorbate/metal system, and molecules which bind irreversibly to Ag, such as organothiols, are not good candidates. Pyridine was chosen because it exhibits a binding strength intermediate between irreversible thiol adsorption and weak adsorption of amines to Ag. In the experiments reported here, excess Lorentzian noise above the $1/f$ background is observed in the PSD when measuring Ag ASJs in pyridine solution. Furthermore, the cutoff frequency varies with solution concentration, but does not depend on the ASJ quantum conductance in the range $G < 8G_0$. Comparing the behavior of 4-aminopyridine to pyridine, the enhanced electron density at the ring N atom produces substantially altered kinetics. Other characteristics of these ASJs, such as the long lifetimes observed in pyridine solution and fluctuations between two metastable quantum conductance states, also illuminate the role of ASJ structural reorganization in mediating the relationship between molecular adsorption and chemical noise in Ag ASJs.

EXPERIMENTAL SECTION

ASJ Fabrication. ASJs are fabricated electrochemically as described previously;[28] however, a few modifications have been introduced in order to assist the observation of surface equilibrium dynamics. Figure 1 shows the equivalent circuit for Ag ASJ formation and subsequent

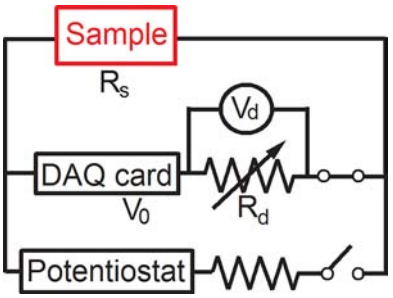

Figure 1. Experimental configuration for ASJ fabrication and noise measurements. Initially the circuit is connected to the potentiostat, which is used as the power source for fabricating ASJs, and then the DAQ card is switched into the system for low-noise fluctuation measurements.

noise measurements. The sample is fabricated on a SiO_2/Si surface onto which two Au electrodes (~100 nm separation) are placed in a tip and anvil configuration. These are used as the template for Ag electroplating and ASJ formation. A fluidic channel constructed in polydimethylsiloxane is placed over the ASJ and connected to a syringe pump for solution delivery. Ag junctions are formed between the gap of two electrodes by potential-controlled electroplating in an electrolyte solution containing 10 μM Ag_2SO_4 and 0.1 M K_2SO_4 (Gamry Instruments, Reference 600). This protocol initially generates overgrown junctions ($G \gg 1G_0$), which are then allowed to self-thin to atomic size by Ag dissolution in the Ag^+-containing electrolyte solution. The rate of self-thinning is controlled, in part, by the Ag^+ concentration. The external resistor to the potentiostat provides for self-termination as, together with the sample junction, it forms a voltage divider to regulate the voltage in the range required for Ag dissolution. The resulting ASJs are stable, typically at several G_0, in both stationary and flowing solution. However, when analyte-containing solution (e.g., pyridine) is delivered to such small junctions, they typically deform and break, causing the observed conductance to drop to zero. To circumvent this problem, analyte solution is delivered to the initially overgrown junction immediately after it is formed. The overgrown junction, being thicker than an ASJ, is sufficiently robust to resist structural failure. Once the analyte solution is admitted, the voltage source is switched to the analog output (AO) of a data acquisition (DAQ) card (National Instrument, PCIe-6361), which

dx.doi.org/10.1021/ja400567j | J. Am. Chem. Soc. 2013, 135, 4522−4528

exhibits much lower electronic noise, and the junction is thinned via electromigration by adjusting the external potentiometer to control the current.

Conductance and Noise Measurements. Conductance and noise measurements are performed by measuring the potential drop across the ballast resistor (V_d) shown in Figure 1, using the analog input (AI) of the DAQ card. A customized Labview program converts the measured voltage data into conductance values and calculates the PSD in real time, allowing both the conductance and the frequency spectrum to be monitored at the same time. Conductance measurements are made at 10 Hz, and the conductance of the sample can be easily computed by

$$G_{\text{sample}}(G_0) = \frac{h}{2e^2}\frac{V_d}{(V_0 - V_d)R_d} \quad (2)$$

The sampling rate for the noise measurement is either 1 or 2 MHz, and 0.1 s of data (100 000 or 200 000 samples) is used to construct a single frequency spectrum. To reduce noise and eliminate individual variations, 100 spectra (10 s) are averaged in Labview and recorded.

Adsorption Measurements. Various concentrations of pyridine, 1 μM < [pyridine] < 10 mM, and 10 μM 4-aminopyridine were prepared in 1:1 (v:v) water−methanol (H_2O−MeOH) mixtures. Absorbance measurements were carried out using a UV−visible spectrometer (Cary 300Bio) to characterize the interactions between pyridine in solution with H_2O−MeOH and a thin Ag film by comparing the absorbance of the pyridine solution before and after exposure to a thermally evaporated Ag thin film in solution.

RESULTS AND DISCUSSION

Fabrication of Atom-Scale Junctions by Electromigration. Previously Au−Ag−Au bimetallic ASJs were fabricated electrochemically, thereby controlling the deposition/dissolution dynamics of Ag at nanoelectrodes and allowing overgrown Ag junctions to self-thin to atomic size.[28] However, when ASJs fabricated this way are exposed to pyridine, the ASJ invariably breaks. We hypothesized that the instability may result from adsorbate-induced structural deformation and eventual failure. Thus, instead of introducing pyridine solution to the fragile ASJ after thinning, we delivered the adsorbate-containing solution (pyridine in 1:1 H_2O−MeOH, but *no* electrolyte) to the initially formed overgrown junction, which remains stable upon pyridine adsorption. Without an electrolyte, electrochemical thinning is dramatically slowed, to the point that electromigration can be used as an attractive junction thinning alternative.

After pyridine is introduced to the overgrown junction, the thinning process is initiated by tuning the external potentiometer to control the current in the QW, thereby inducing electromigration. Figure 2 shows a typical conductance vs time trace measured by the DAQ card for junction thinning by electromigration. The spikes occur when the potentiometer is adjusted (manually) to control the rate of thinning. The resistance of the potentiometer is controlled between 50 Ω and 5 kΩ. At $t \approx 8500$ s, the conductance abruptly plummets from $\sim 20G_0$ to $1G_0$ and remains stable for a very long time, >1000 s (see Figure 2 inset).

Electromigration has been widely used to create nanogaps for single-molecule contact studies.[29−31] In the present experiments, electromigration-induced thinning is rapid when the junction is in the diffusive electron transport regime, $G > 20\ G_0$, due to high current density and high effective electron temperature in the junction.[32,33] When the junction shrinks to atomic size ($<10G_0$), the bulk of the electron transport is in the ballistic regime, so that nanoscale heating, which governs ionic movement resulting in electromigration, is much

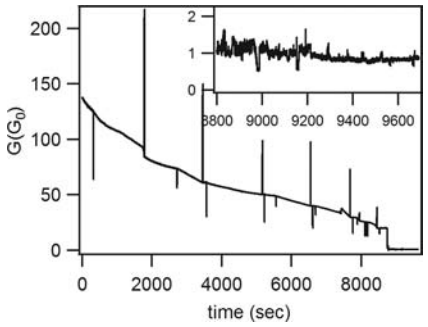

Figure 2. Typical conductance vs time trace after the circuit is switched to thinning mode. Junction thinning is then performed by adjusting the potentiometer (spikes) to control the current that induces electromigration. (Inset) Junction stabilized at $G \approx 1G_0$ for an extended period (~15 min).

lower.[32,33] The biggest challenge encountered in using electromigration to fabricate ASJs is the survival rate of ASJs after the accelerated thinning in the diffusive transport regime. The likelihood of breaking the junction is high, and there are no standard criteria for controlling the potentiometer or the voltage source to maintain stable ASJs. However, the "bimetallic" scheme used here provides a robust template that allows repeatable junction formation on one sample, which greatly reduces fabrication time. Moreover, it is observed that the presence of an adsorbate (pyridine) greatly increases the success rate of stable ASJs formation. This can be explained by the lower surface energy of ASJs after molecular adsorption,[34−36] as discussed below.

Surface Fluctuation Spectroscopy. The electrical signal measured in a sensing experiment contains several noise components: Johnson−Nyquist noise generated by the thermal agitation of the charge carriers, $1/f$ noise stemming from resistance fluctuations, instrument noise, and the noise source of interest here, noise caused by chemical dynamics, i.e., molecular adsorption and desorption. Chemical noise is observed in the conductance signal due to adsorbate-induced scattering, which results in a coverage-dependent conductance, $G(N)$. Thus, fluctuations in coverage, δN, produce corresponding fluctuations in conductance, δG. In order to observe the chemical noise, its magnitude must be greater than, or comparable to, the total magnitude of the noise from all other sources. In this sense, ASJs are perfect candidates to study chemical noise, because they exhibit high resistance ($R_0 = 1/G_0 \approx 12.9$ kΩ), and the normalized resistance change ($\Delta R/R_0$) due to adsorption of a few molecules (N) is also large. Therefore, the resistance fluctuations associated with molecular fluctuations at equilibrium, which scale as $\Delta R/\sqrt{N}$, are also large. A simple relationship between the chemical noise of the measured signal, δV_{dI}, and the chemical-induced resistance fluctuation, δR_{dI}, for the circuit shown in Figure 1 is given by

$$\delta V_{dI} = -\frac{V_0 R_d}{(R_d + R_s)^2}\delta R_{dI} \quad (3)$$

From this equation, it is clear that the resistance of the potentiometer, R_d, and the voltage, V_0, driving current flow in the circuit both play important roles in achieving chemical noise-related signals, δV_{dI}, of sufficient magnitude to be measurable. In the equilibrium fluctuation experiments, optimal settings of V_0 between 0.4 and 0.5 V, and R_d between 2 and 5 kΩ, generate distinguishable chemical noise signals.

dx.doi.org/10.1021/ja400567j | J. Am. Chem. Soc. 2013, 135, 4522−4528

For a simple reversible reaction system, Feher and Weissman showed that the relationship between the chemical population fluctuations at equilibrium, δN, and their frequency spectrum or PSD[21] is given by

$$\langle \delta N(f)^2 \rangle = \frac{4\tau \langle N \rangle (1 - \langle N \rangle / N_T)}{1 + (2\pi f \tau)^2} \quad (4)$$

where N_T is the total population, which contains N molecules of the species of interest, and τ is the chemical relaxation time. This relation produces a Lorentzian noise function, with a characteristic cutoff frequency $f_c = (2\pi\tau)^{-1}$. A surface with an adsorbed population in equilibrium can be described by this relation, so the frequency spectrum of the surface population fluctuations should also be Lorentzian. Furthermore, for a small perturbation, the relationship of the chemical-induced resistance fluctuation and the population fluctuation is $\delta R_{dI} = (\partial R/\partial N)\delta N$, and it can be assumed that each molecule contributes equally to a resistance change, i.e., $(\partial R/\partial N)$ is constant. In eq 3, δV_{dI} is proportional to δR_{dI}, so in the PSD obtained from the measured signal, the component related to chemical fluctuations should be Lorentzian.

In an electrical circuit containing an ASJ, the dominant noise contribution at low frequencies is $1/f$ noise,[37,38] since the Johnson–Nyquist noise arising from dissipative processes[39] is much smaller than the $1/f$ noise magnitude. Chemical noise thus produces a Lorentzian component in addition to the inherent $1/f$ component. Figure 3a illustrates how the noise components are ideally related by showing simulated $1/f$ noise, Lorentzian noise (f_c = 30 kHz), and the sum of both components in an amplitude (dB) vs frequency log–log plot.

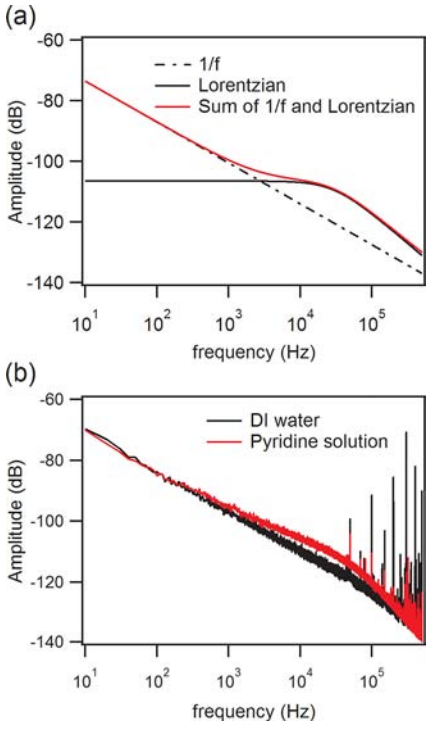

Figure 3. (a) Simulated noise signals showing the relative shapes of different noise components. $1/f$ noise dominates at low frequency; the Lorentzian function represents noise induced by surface adsorbate population fluctuations. (b) Power spectral density of measured signals from Au–Ag–Au bimetallic ASJs in DI water and in 100 μM pyridine in 1:1 H_2O–MeOH.

Lorentzian noise in this format exhibits a plateau at frequencies lower than f_c and a linear decay at $f > f_c$. The presence of a Lorentzian noise component alters the slope of the PSD, and the sum of the $1/f$ and Lorentzian components produces a plot with two inflection points: one where the Lorentzian noise becomes comparable in magnitude to the $1/f$ component, and another at f_c. We note that there is, in principle, additional information in the magnitude of the Lorentzian components, especially their dependence on the kinetics of the surface adsorption/desorption processes giving rise to the chemical noise, but such comparisons are beyond the scope of the present study. In Figure 3b the PSD produced from adsorption of 100 μM pyridine onto a Au–Ag–Au bimetallic ASJ is compared to the PSD in deionized (DI) water. It is clear that the presence of pyridine in solution produces an excess noise component relative to the pure $1/f$ noise measured in DI water. The excess noise component has a Lorentzian spectral signature and can be assigned to adsorbed pyridine population fluctuations.

To investigate the molecular origins of the excess noise in the PSD, data were analyzed using a simple Langmuir adsorption model, in which the relaxation time, τ, is related to the adsorption and desorption kinetics by $1/\tau = k_a C_A + k_d$, where k_a and k_d are the rate constants for adsorption and desorption, respectively, and C_A is the adsorbate (solution) concentration. Further, τ is related to the Lorentzian noise component by $f_c = (2\pi\tau)^{-1}$. These relationships suggest that if C_A is increased, f_c should shift to higher frequencies. To test this hypothesis, a series of solutions with varying pyridine concentrations between 1 μM and 10 mM was tested, viz. Figure 4a. Clearly, f_c increases with concentration. Details of the curve fitting and data development are given in the Supporting Information.

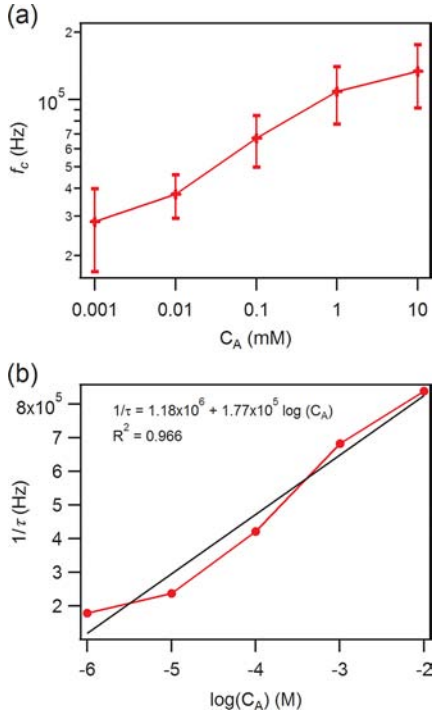

Figure 4. (a) Log–log plot of cutoff frequency, f_c, vs pyridine concentration. Error bars correspond to ±1 standard deviation from replicate experiments, and the points are connected by line segments as a guide to the eye. (b) Plot of $1/\tau$ vs log [pyridine]. Solid black line represents a fit to a linear model.

dx.doi.org/10.1021/ja400567j | J. Am. Chem. Soc. 2013, 135, 4522–4528

However, relaxation time does not respond to the concentration change exactly as predicted, cf. Figure 4b. Instead, it is found that $1/\tau$ (Hz) = $(1.18 \times 10^6) + (1.77 \times 10^5)\log(C_A)$, indicating that $1/\tau$ is linearly related to $\log(C_A)$ instead of C_A. This implies that the actual adsorption mechanism for adsorption of pyridine on Ag ASJ surfaces is more complicated than the simple Langmuir model over the range of pyridine concentrations examined.

The pyridine–Ag adsorption isotherm has been measured by surface-enhanced Raman scattering,[40] and the concentration range used here spans the whole isotherm, from ~1 μM, where pyridine just starts to adsorb, up to 10 mM, where pyridine fully saturates the surface. In order to calculate k_a and k_d and the corresponding adsorption free energy, $\Delta G_{ads} = -RT \ln K$, where $K = k_a/k_d$, the $1/\tau$ function is fit at each pair of adjacent concentrations The results are listed in Table 1. The kinetic

Table 1. Calculated Kinetic (k_a, k_d) and Thermodynamic (ΔG_{ads}) Parameters

C_A (M)	$1/\tau$ (s^{-1})	k_a (M^{-1} s^{-1})	k_d (s^{-1})	ΔG_{ads} (kJ mol^{-1}) at 300 K
10^{-6}	178 000			
		6.54×10^9	1.72×10^5	−26.3
10^{-5}	237 000			
		2.05×10^9	2.16×10^5	−22.8
10^{-4}	421 000			
		2.90×10^8	3.92×10^5	−16.5
10^{-3}	683 000			
		1.73×10^7	6.65×10^5	−8.13
10^{-2}	838 000			

parameters change with concentration: k_a decreases while k_d increases, and ΔG_{ads} becomes less energetically favorable, as pyridine concentration increases. In the Langmuir model, k_a and k_d are assumed to be coverage independent, while more general expressions for adsorption kinetics include coverage-dependent activation energies of adsorption and desorption.[41] Clearly, surface coverage significantly affects the kinetics for pyridine adsorption at atomic-scale Ag features. $\Delta G_{ads} = -22.8$ kJ mol^{-1}, calculated from data in the concentration range 10–100 μM, is in good agreement with a previously reported value, −24 kJ mol^{-1},[40] in the same concentration range as well as other literature values, −20.1 to −21.8 kJ mol^{-1}.[42] The coverage dependence of ΔG_{ads} that characterizes pyridine adsorption at Ag ASJs can likely be ascribed to the fact that the surface sites available for molecular adsorption at ASJs are not equivalent, a possibility discussed by Green and Liu in considering how Ag nanoring architectures give rise to SERS signals. If the sites are inequivalent, producing a distribution, $N(E_b)$, with site energies, E_b, then the strongest binding sites should be occupied first, i.e., at lowest solution concentrations, in accord with the observed trend of ΔG_{ads} with pyridine concentration given in Table 1.

Clearly, the cutoff frequency, f_c, shifts with pyridine concentration, as anticipated. To understand how the chemical noise changes when the electronic structure of the adsorbate changes, a series of experiments was performed with 4-aminopyridine. The measured f_c for 10 μM 4-aminopyridine is 101 ± 20.2 kHz (Figure S3), compared to 37 ± 8.3 kHz (see Figure 4a) for 10 μM pyridine. Since attaching an electron-donating amine to the *para* position in pyridine increases the electron density at the pyridine N atom, the metal–N interaction increases. Indeed, normal coordinate analysis shows that the metal–nitrogen bond strength, as reflected in the metal–nitrogen vibrational frequency in metal–ligand complexes, is sensitive to the electron-withdrawing/donating effect of ligands in the *para* position of the pyridine ring.[43] Thus, given the expected enhancement in binding strength, the higher cutoff frequency likely points to faster adsorption kinetics for 4-aminopyridine on the Ag ASJ than for pyridine.

Given the putative role of the Ag ASJ surface site distribution in determining the concentration dependence of f_c, it is reasonable to ask whether the size of the ASJ affects the adsorbate kinetics. In typical experiments, it is very difficult to control the exact size of the junction, so PSD data were captured at ASJs of different junction sizes, exhibiting conductances in the range $G < 8G_0$. Figure 5a shows a

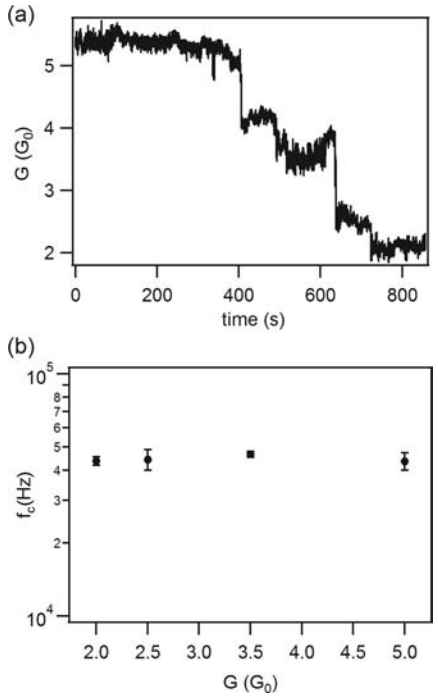

Figure 5. (a) Conductance versus time trace of ASJ at different conductance plateaus. (b) The cutoff frequencies corresponding to the different conductance plateaus in (a).

conductance vs time trace for an ASJ undergoing spontaneous thinning through several discontinuous steps in conductance from $5G_0$ to $2G_0$ in the presence of pyridine in H_2O–MeOH. PSD data were collected at different plateaus to see how f_c varies with junction size (see Figure S4). As is evident from Figure 5b, the junction size does not affect the molecular relaxation time. Therefore, PSD data recorded at ASJs of different sizes in the conductance range $<8G_0$ reflect the same molecular adsorption/desorption dynamics and the same underlying $N(E_b)$ surface site distributions. Some ASJs exhibit conductance which fluctuates between two stable conductance states (*vide infra*), likely reflecting junction reorganization between two metastable states. In these cases the time-averaged PSD data are influenced by several factors: (a) $1/f^\alpha$ noise, with different α values for different size AJSs,[37] (b) Lorentzian junction reorganization, which may exhibit a different cutoff frequency than molecular adsorption/desorption,[44] and (c) chemical noise from the adsorbate, which is still present. This behavior, while inherently interesting, produces time-averaged

dx.doi.org/10.1021/ja400567j | J. Am. Chem. Soc. 2013, 135, 4522–4528

PSD data which cannot be easily interpreted at present. Thus, all PSD data presented in this work were recorded at stable (≥20 s) ASJ conductance states.

Molecular Adsorption Effects on ASJ Conductance Fluctuations. Interestingly, Au−Ag−Au bimetallic junctions fabricated by the overgrowth-thinning strategy in 1:1 H_2O−MeOH can only endure the thinning process in the presence of pyridine concentrations $C_A \geq 100$ nM. When pyridine is absent, the vast majority of thinning junctions simply break to produce a nanogap. To learn more about the effect of pyridine on the structural reorganization dynamics of Ag ASJs, UV absorption measurements were performed on 10 μM pyridine in 1:1 H_2O−MeOH, in the presence and absence of a Ag thin film (thin film not in the beam path), Figure 6. First, a reference spectrum was obtained for 10 μM pyridine in 1:1 H_2O−MeOH (Figure 6, red). A 100 nm thermally evaporated Ag thin film was then immersed in the solution (2 mL) for 30 min, after which another UV absorption spectrum was obtained (Figure 6, blue). After the Ag film was placed in solution, the absorption increased in the range 210 nm < λ < 240 nm, presumably from the low-energy tail of a higher energy transition. Comparing this to the absorption spectrum from a Ag substrate inserted into solution in the absence of pyridine (Figure 6, black) reveals the same absorption tail. Clearly, pyridine adsorption to Ag cannot account for the increase in solution absorbance, since pyridine would be removed from solution. Furthermore, the 10 μM pyridine spectrum shows no absorption in the 210−225 nm window, although there is clearly a separate high-energy solvent absorption in the 200−210 nm window. The band tail observed for the Ag film contact with MeOH−H_2O in the absence of pyridine cannot be assigned definitively, but it is similar in strength and position to a band tail absorption observed for 70 nm Ag colloids[45] and to the products obtained by long-term pulse radiolysis of Ag clusters.[46] Evidently the Ag thin film interacts with H_2O−MeOH to produce absorbing species in solution, possibly by stripping off in small Ag clusters, thereby enhancing the absorbance of the solution. This helps explain why ASJ fabrication is unsuccessful in pure H_2O−MeOH and at very low concentrations of pyridine ($C_A \leq 100$ nM) but is successful at higher concentrations. We hypothesize that higher pyridine concentrations stabilize Ag ASJ junctions by increasing the energy needed for Ag atom reorganization in the junction. Indeed, Au−Ag−Au ASJs can be very stable in pyridine solution. For example, Figure 7a shows an ASJ which remains at ~$3G_0$ for more than 20 min.

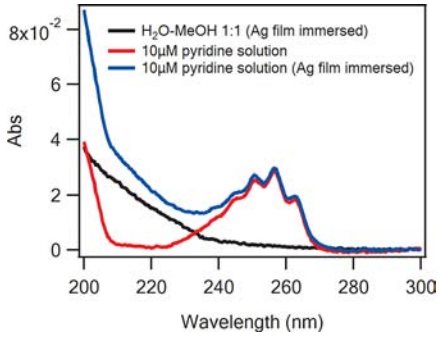

Figure 6. UV spectra of 10 μM pyridine solution before and after a Ag film is immersed in the solution: 10 μM pyridine in 1:1 H_2O−MeOH, no Ag (red); 10 μM pyridine in 1:1 H_2O−MeOH, in the presence of Ag thin film (blue); 1:1 H_2O−MeOH in the presence of Ag thin film, no pyridine (black). The transition at 258 nm with vibrational fine structure is the pyridine n→π* transition.[48]

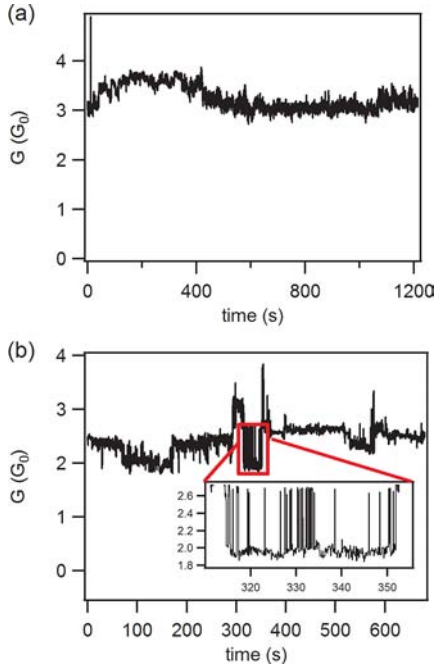

Figure 7. Conductance traces in the presence of 10 μM 4-aminopyridine. (a) Long lifetime ASJ stable at ~$3G_0$. (b) ASJ exhibiting conductance fluctuating between two stable levels. (Inset) Magnified view of two-level fluctuations.

In some cases ASJ conductance fluctuates rapidly between two stable states. For example, Figure 7b shows conductance fluctuating between ~$2G_0$ and $2.7G_0$ in the presence of 10 μM 4-aminopyridine. Several groups have reported this kind of two-level fluctuation in metal nanobridges at low (<150 K) temperature,[44,47] attributing the phenomenon to reversible motion of an atomic-scale defect quenched at low temperature between two metastable states. In the present case, the two-level fluctuations are observed only in the presence of molecular adsorbate—both pyridine and 4-aminopyridine—since the junctions typically break to form nanogaps in the absence of the adsorbate. Although the rapid conductance fluctuations prevent us, at present, from analyzing the adsorption/desorption behavior in these time windows, it is quite likely that the same underlying structural phenomena are responsible for both the stabilization of Ag ASJs in the presence of Lewis base adsorbates and the metastable conductance states causing the two-level conductance fluctuations. Further investigation of this two-level fluctuation and its dependence on the nature of the adsorbate is proceeding.

■ CONCLUSIONS

Au−Ag−Au bimetallic ASJs can be successfully fabricated at high yield using a combined electrochemical deposition/electromigration thinning approach. Thinning is carried out in the presence of an adsorbate, e.g., pyridine, which stabilizes the ASJ sufficiently that it can be stopped at stable low-conductance states, $G < 10G_0$, although electromigration rarely produces a stable low-conductance junction in the absence of a stabilizing adsorbate. In measurements of the electrical conductance of ASJs in the presence of pyridine, noise

dx.doi.org/10.1021/ja400567j | J. Am. Chem. Soc. 2013, 135, 4522−4528

corresponding to molecular fluctuations of the adsorption/desorption equilibrium is enhanced due to the relatively large resistance (R > 1.6 kΩ) of the ASJs and the small populations that can adsorb on the surface. Such chemical noise is characterized by a Lorentzian function in the frequency spectrum with a cutoff frequency that shifts with the kinetics of the adsorption/desorption process. Therefore, characteristic variations in the frequency position of the Lorentzian are observed with increasing concentration of pyridine solutions, or by switching to adsorbates, like 4-aminopyridine, with different binding characteristics. While the adsorption free energy of pyridine to Ag calculated from fluctuation measurements is in good agreement with literature values at comparable concentrations (10 μM), the adsorption free energy is observed to become less favorable with increasing pyridine concentration. This observation is likely related to the presence of inequivalent adsorption sites and shifts in Ag electronic structure at the nanoscale. These observations indicate that the atomic-scale dynamics of junction reordering are fundamentally altered by the presence of a Lewis base adsorbate, like pyridine, and that the application of fluctuation spectroscopy to characterize chemical noise at mesoscopic junctions is a fruitful approach to the study of adsorbate−metal interactions in these nanoscale systems, revealing kinetic information embedded within the chemical noise caused by molecular fluctuations at equilibrium.

■ ASSOCIATED CONTENT

Supporting Information

Detailed description of the fitting protocol used to elucidate the positions of the Lorentzian noise components. This material is available free of charge via the Internet at http://pubs.acs.org.

■ AUTHOR INFORMATION

Corresponding Author

pbohn@nd.edu

Notes

The authors declare no competing financial interest.

■ ACKNOWLEDGMENTS

This work was supported by the National Science Foundation through grant 1111739 (support of T.-W.H.) and through the Center for Advanced Materials for Water Purification with Systems, cooperative agreement 0120978 (support of S.P.B.).

■ REFERENCES

(1) Persson, B. N. J.; Schumacher, D.; Otto, A. *Chem. Phys. Lett.* **1991**, *178*, 204.
(2) Zhang, Y. M.; Terrill, R. H.; Bohn, P. W. *Anal. Chem.* **1999**, *71*, 119.
(3) McCullen, E. F.; Hsu, C. L.; Tobin, R. G. *Surf. Sci.* **2001**, *481*, 198.
(4) Fahsold, G.; Sinther, M.; Priebe, A.; Diez, S.; Pucci, A. *Phys. Rev. B* **2004**, 70.
(5) Hein, M.; Schumacher, D. *J. Phys. D* **1995**, *28*, 1937.
(6) Murray, B. J.; Walter, E. C.; Penner, R. M. *Nano Lett.* **2004**, *4*, 665.
(7) Jihoon, K.; Hyungcheoul, S.; Donghyun, L.; Kyungsoo, K.; Jinhwan, L.; Kyungsoo, K.; Soohyun, K. *10th IEEE Conference on Nanotechnology (IEEE-NANO)*, 2010; p 753.
(8) Shi, P.; Zhang, J. Y.; Lin, H. Y.; Bohn, P. W. *Small* **2010**, *6*, 2598.
(9) Fuchs, K. *Math. Proc. Cambridge Philos. Soc.* **1938**, *34*, 100.
(10) Sondheimer, E. H. *Adv. Phys.* **1952**, *1*, 1.
(11) Tao, N. J. *J. Chem. Educ.* **2005**, *82*, 720.
(12) Agrait, N.; Yeyati, A. L.; van Ruitenbeek, J. M. *Phys. Rep.* **2003**, *377*, 81.
(13) Li, C. Z.; He, H. X.; Bogozi, A.; Bunch, J. S.; Tao, N. J. *Appl. Phys. Lett.* **2000**, *76*, 1333.
(14) Bogozi, A.; Lam, O.; He, H. X.; Li, C. Z.; Tao, N. J.; Nagahara, L. A.; Amlani, I.; Tsui, R. *J. Am. Chem. Soc.* **2001**, *123*, 4585.
(15) Leroux, Y. R.; Fave, C.; Zigah, D.; Trippe-Allard, G.; Lacroix, J. C. *J. Am. Chem. Soc.* **2008**, *130*, 13465.
(16) Dong, X.; Liu, J.; Zhang, B.; Xia, Y. *Electrochim. Acta* **2012**, *74*, 78.
(17) Zhang, Y.; Terrill, R. H.; Bohn, P. W. *Anal. Chem.* **1999**, *71*, 119.
(18) Castle, P. J.; Bohn, P. W. *Anal. Chem.* **2005**, *77*, 243.
(19) Donnan, F. G.; Teller, E.; Topley, B. *Philos. Mag.* **1937**, *24*, 981.
(20) Duan, B. K.; Zhang, J.; Bohn, P. W. *Anal. Chem.* **2011**, *84*, 2.
(21) Feher, G.; Weissman, M. *Proc. Natl. Acad. Sci. U.S.A.* **1973**, *70*, 870.
(22) Weissman, M. B. *Annu. Rev. Phys. Chem.* **1981**, *32*, 205.
(23) Zevenbergen, M. A. G.; Singh, P. S.; Goluch, E. D.; Wolfrum, B. L.; Lemay, S. G. *Anal. Chem.* **2009**, *81*, 8203.
(24) Fan, F. R. F.; Kwak, J.; Bard, A. J. *J. Am. Chem. Soc.* **1996**, *118*, 9669.
(25) Hoogerheide, D. P.; Garaj, S.; Golovchenko, J. A. *Phys. Rev. Lett.* **2009**, 102.
(26) De, G. S.; Suhl, H. *Surf. Sci.* **1980**, *95*, 67.
(27) Zheng, G. F.; Gao, X. P. A.; Lieber, C. M. *Nano Lett.* **2010**, *10*, 3179.
(28) Hwang, T.-W.; Bohn, P. W. *ACS Nano* **2011**, *5*, 8434.
(29) Park, J.; Pasupathy, A. N.; Goldsmith, J. I.; Chang, C.; Yaish, Y.; Petta, J. R.; Rinkoski, M.; Sethna, J. P.; Abruna, H. D.; McEuen, P. L.; Ralph, D. C. *Nature* **2002**, *417*, 722.
(30) Park, H.; Lim, A. K. L. *Appl. Phys. Lett.* **1999**, *75*, 301.
(31) Mahapatro, A. K.; Ghosh, S.; Janes, D. B. *IEEE Trans. Nanotechnol.* **2006**, *5*, 232.
(32) Taychatanapat, T.; Bolotin, K. I.; Kuemmeth, F.; Ralph, D. C. *Nano Lett.* **2007**, *7*, 652.
(33) Hoffmann, R.; Weissenberger, D.; Hawecker, J.; Stoffler, D. *Appl. Phys. Lett.* **2008**, *93*, 043118.
(34) He, H. X.; Shu, C.; Li, C. Z.; Tao, N. J. *J. Electroanal. Chem.* **2002**, *522*, 26.
(35) Kiguchi, M.; Konishi, T.; Murakoshi, K. *Appl. Phys. Lett.* **2005**, *87*, 043104.
(36) Kiguchi, M.; Miura, S.; Murakoshi, K. *Surf. Sci.* **2007**, *601*, 4127.
(37) Wu, Z.; Wu, S.; Oberholzer, S.; Steinacher, M.; Calame, M.; Schönenberger, C. *Phys. Rev. B* **2008**, *78*, 235421.
(38) Bid, A.; Bora, A.; Raychaudhuri, A. K. *Nanotechnology* **2006**, *17*, 152.
(39) Johnson, J. B. *Phys. Rev.* **1928**, *32*, 97.
(40) Green, M.; Liu, F. M. *J. Phys. Chem. B* **2003**, *107*, 13015.
(41) Tsay, R. Y.; Lin, S. Y.; Lin, L. W.; Chen, S. I. *Langmuir* **1997**, *13*, 3191.
(42) Chen, C. K.; Heinz, T. F.; Ricard, D.; Shen, Y. R. *Chem. Phys. Lett.* **1981**, *83*, 455.
(43) Topacli, A.; Bayari, S. *Spectrochim. Acta A* **2001**, *57*, 1385.
(44) Holweg, P. A. M.; Caro, J.; Verbruggen, A. H.; Radelaar, S. *Phys. Rev. B* **1992**, *45*, 9311.
(45) Kämmer, E.; Dörfer, T.; Csáki, A.; Schumacher, W.; Da Costa Filho, P. A.; Tarcea, N.; Fritzsche, W.; Rösch, P.; Schmitt, M.; Popp, J. *J. Phys. Chem. C* **2012**, *116*, 6083.
(46) Jacob, J. A.; Kapoor, S.; Biswas, N.; Mukherjee, T. *Colloids Surf. A* **2007**, *301*, 329.
(47) Ralls, K. S.; Ralph, D. C.; Buhrman, R. A. *Phys. Rev. B* **1989**, *40*, 11561.
(48) Hochstrasser, R. M. *Acc. Chem. Res.* **1968**, *1*, 266.